Available online at www.sciencedirect.com
ScienceDirect
Acta Materialia 56 (2008) 2456–2468
Acta MATERIALIA
www.elsevier.com/locate/actamat

Reorientation and stress relaxation due to twinning: Modeling and experimental characterization for Mg

B. Clausen [a,*], C.N. Tomé [b], D.W. Brown [b], S.R. Agnew [c]

[a] LANSCE-LC, Los Alamos National Laboratory, Los Alamos, NM 87545, USA
[b] MST-8, Los Alamos National Laboratory, Los Alamos, NM 87545, USA
[c] Materials Science and Engineering, University of Virginia, Charlottesville, VA 22904, USA

Received 16 August 2007; received in revised form 17 January 2008; accepted 18 January 2008
Available online 18 April 2008

Abstract

A study of the mechanical response of Mg AZ31 when deformed under twinning dominated conditions is presented. In addition to the well-known rapid texture variation, neutron diffraction measurements reveal a 'sense-reversal' of the internal stress in the twinned grains. The latter is characterized experimentally and an elasto-plastic polycrystal model is extended in order to account for twin domain reorientation and associated stress relaxation. It is concluded that the texture variation due to twinning is sufficient to explain the observed macroscopic stress–strain response. However, the evolution of internal stresses in diffracting subsets of grains is complex and more challenging to explain. It seems to be strongly controlled by the order in which slip and twinning are activated, the stress relaxation associated with twin propagation, and neighbor constraint effects.

Keywords: Neutron diffraction; Magnesium alloys; Twinning; Texture; Elastic–plastic self-consistent (EPSC) model

1. Introduction

Mg alloys are unique systems because tensile twinning and de-twinning can be easily activated, which leads to rapid texture and hardening evolution [1]. While the role of twinning on such processes is qualitatively understood, quantitatively predictive capabilities have lagged behind. Visco-plastic self-consistent (VPSC) polycrystal deformation models [2,3] have recently been extended to describe simultaneously twin and hardening evolution in Zr and Mg, including de-twinning effects [1,4,5]. VPSC models, however, do not account for hydrostatic stresses or for the elastic deformation component, and cannot be used to study internal stress evolution. Elasto-plastic self-consistent (EPSC) polycrystal models [6–8], in contrast, account for elastic effects but usually not for (i) twin activation, (ii) twin reorientation (and the associated texture evolution), and (iii) the specific stress relaxation associated with twinning (as opposed to that of slip). Both models use the Eshelby inclusion approach [9] to represent the interaction of each grain (treated as an ellipsoidal inclusion) with a homogenous equivalent medium (HEM) which has the average properties of the polycrystal. In fact, no direct grain-to-grain interaction is addressed but, rather, the average response of each orientation with an averaged neighborhood.

The models described above are based upon grain-level deformation mechanisms of dislocation slip and mechanical twinning and, hence, provide information about the deformation behavior on the scale of the grains. This level of detail matches well the information provided by bulk experimental diffraction techniques, such as neutron or synchrotron X-ray. Within these techniques, the measured data represent an average of many grains with similar orientation but with different surroundings, resulting in the same level of detail as the effective field models provide. Hence, the one-site self-consistent models and bulk

* Corresponding author. Tel.: +1 505 667 2944; fax: +1 505 665 2676.
E-mail address: clausen@lanl.gov (B. Clausen).

1359-6454/$34.00
doi:10.1016/j.actamat.2008.01.057

diffraction techniques have successfully been used in combination to develop and validate constitutive models using diffraction measurements for simple deformation histories [10,11], and then to interpret the diffraction data for more complex cases [12,13].

Here, an extension of the EPSC model is presented which aims to address the three limitations (activation, reorientation and relaxation) described above in what concerns the treatment of twinning. What motivates this extension is the need to interpret the measured response of extruded Mg deforming in compression along the extrusion axis. The extrusion process results in the so-called 'rod texture', where the basal poles of most grains are oriented at an angle of nearly 90° to the extrusion direction. In a previous study, the EPSC approach was applied to analyzing the tensile response of this material [14], as little twinning takes place during axial tension. However, in the case of axial compression, almost all the grains are favorably oriented for activating tensile twinning, which leads to significant texture changes as the twinned part of a grain is reoriented by ~86.6°.

As a consequence, the extended model must include texture development and stress relaxation due to twinning. In situ neutron diffraction measurements of elastic lattice strain and bulk texture evolution will be used, as well as macroscopic measurements of stress–strain response to test/validate the model predictions. In turn, the combined use of both neutron diffraction and polycrystal deformation models provides basic understanding of crystallographic mechanisms, as will be shown in this work for the specific case of twinning.

2. New twinning scheme for the EPSC model

In the following, a twinning scheme and its implementation into the EPSC deformation model is described. Within the EPSC model (see Ref. [7] for a detailed description), the polycrystal is represented as a collection of crystal orientations with volume fractions chosen to reproduce the known initial texture. Each grain is treated as an ellipsoidal elasto-plastic inclusion embedded in the HEM representing the aggregate. The properties and macroscopic response of the HEM are calculated via weighted averages over all the grains. The incremental constitutive response of the grain is

$$\delta\sigma^g = C^g : \left(\delta\varepsilon^{g,\text{total}} - \sum_s m^{g,s}\delta\gamma^s\right) \tag{1}$$

where $\delta\sigma^g$ is the stress increment, C^g is the fourth rank elastic stiffness tensor, $\delta\varepsilon^{g,\text{total}}$ is the total (elastic + plastic) strain increment, and $m^{g,s}$ is the Schmid tensor, which resolves the shear strain increment $\delta\gamma^s$ contributed by the slip or twinning system s. This is, in fact, an implicit non-linear constitutive law, where the slip/twin shears also depend upon the stress increment. The current EPSC approach uses the same condition for twin activation as for slip activation, namely a Schmid law which requires the resolved shear stress on the twin or slip plane in the slip or twin direction to exceed a critical value, τ^s:

$$\tau^s = m^{g,s} : \sigma^g \tag{2}$$

Further, the resolved shear stress must remain at the critical value throughout a straining step as the material strain hardens:

$$\delta\tau^s = m^{g,s} : \delta\sigma^g \tag{3}$$

Here, twin nucleation is not accounted for, which is assumed to take place through stress concentration mechanisms at such a local level as to be unresolvable by this mesoscopic/grain-level model. The EPSC model incorporates an extended Voce hardening rule for the evolution of τ^s with total accumulated plastic strain within the grain Γ:

$$\tau^s = \tau_0^s + (\tau_1^s + \theta_1^s\Gamma)\left(1 - \exp\left(-\frac{\theta_0^s\Gamma}{\tau_1^s}\right)\right) \tag{4}$$

These single crystal (grain-level) constitutive laws can be linearized as follows [15]:

$$\delta\sigma^g = L^g : \delta\varepsilon^{g,\text{total}} \tag{5}$$

where L^g is the elasto-plastic stiffness of the grain, which is a function of the elastic moduli and the active slip and twin systems. Similarly, the incremental response of the effective medium is

$$\delta\bar{\sigma} = \overline{L} : \delta\bar{\varepsilon}^{\text{total}} \tag{6}$$

where the tensors have the same meaning as in Eq. (5) but the overbars refer to the polycrystalline effective medium rather than the individual grain, g. The response of each grain follows from solving the stress equilibrium and compatibility relations for an inclusion embedded in a homogeneous medium whose constitutive responses are described by Eqs. (5) and (6), respectively. The condition that the average of the grain increments has to be equal to the macroscopic increments

$$\delta\bar{\sigma} = \langle\delta\sigma^g\rangle \quad \text{and} \quad \delta\bar{\varepsilon} = \langle\delta\varepsilon^g\rangle \tag{7}$$

leads to a 'self-consistent' equation for the macroscopic elasto-plastic stiffness $\overline{L}$. Once the elasto-plastic stiffness $\overline{L}$ is found for a given step, the macroscopic stress increment associated with an imposed strain increment $\delta\bar{\varepsilon}^{\text{total}}$ is given by Eq. (6) and the new stress state is found as

$$\bar{\sigma} = \bar{\sigma} + \delta\bar{\sigma} \tag{8}$$

To this point, everything about the current model follows the original implementation [7]. In the extended EPSC scheme, activation and relaxation are considered in detail, and there is the additional major issue involving the fact that a new 'child' grain must be 'created' when a twin system becomes active in the initial 'parent' grain. The orientation of these new grains is easily determined from the crystallographic relation between the parent and twin. Each parent grain can have multiple twin 'children', one

for each active twin system. The children are allowed to grow as further twin activity takes place and, in the process, some volume fraction is transferred from the parent to the child, while keeping the total volume fraction constant and equal to the initial volume fraction of the parent grain. (This section refers to volume fractions relative to the initial parent. In the simulations, each parent and child has associated an absolute volume fraction which is the one used for performing polycrystal averages.) The increment in the twin volume δw^t fraction for each twin t is given by

$$\delta w^t = \frac{\delta \gamma^t}{S^t} \tag{9}$$

where $\delta \gamma^t$ is the shear increment contributed by the twin system t of the parent grain, and S^t is the characteristic twin shear (for tensile twins in Mg $S^t = 0.130$ [16]). Hence, the change in the parent volume fraction δw^{parent} is given by the sum over all active twin systems:

$$\delta w^{\text{parent}} = -\sum_t \delta w^t \tag{10}$$

In the EPSC simulation, the changes in the volume fractions are imposed at the end of each strain increment. It is important to note that, after it has been created, the twin is treated as a new independent grain, and the only coupling between child and parent is through the volume transfer. Such assumption is reasonable once the twin has grown to be comparable in size with the parent grain. In the case of axial compression of extruded Mg considered here, ~70% of the aggregate twins after 10% compression. Contrary to the predominant twin reorientation scheme [1] or the Composite Grain model scheme [4,5] used in the VPSC model, there is no threshold for reorientation; rather, the parents are allowed to split into more than one twin orientation, and there is no limit on the maximum fraction of twinning. As a matter of fact, a parent can be fully consumed by twinning and disappear, i.e., its weight goes to zero.

Even at this point in the discussion, the underlying theory of the EPSC model remains the same [7], and the only addition is the bookkeeping required to keep track of the evolving relative fractions of parents and twins, and the numerical burden of considering up to six possible twin variants for each initial orientation. However, two complications arise, which require specific attention. As mentioned earlier, the macroscopic stresses are updated according to self-consistency and strain hardening condition given by Eqs. (7) and (8). However, as the weights of the grains are varied and new grains are introduced at the end of each step, the overall stress and strain increments given by Eq. (7) are modified. The relative difference is small (typically <0.5% at the macroscopic level) but, to avoid accumulation of errors, the macroscopic values are updated using the recalculated averages over the grains after the volume fractions are updated according to Eqs. (9) and (10).

Thus, as the newly created twins enter the calculations with non-zero weight, an initial stress and strain state must be assigned to them. Local simulations of twin formation would help elucidate this issue but are beyond the aim of the present work. However, assumptions made here are consistent with recent finite element (FE) method predictions of the local stress and strain development during twinning [17]. One way of estimating the initial stress and elastic strain state in the new twin is to apply continuity assumptions for tractions and displacements across the twin boundary, respectively. It is worth noting that, while the grain stress and strain are assumed uniform in the EPSC model, in reality there will be gradients inside the grains. However, at inception, the twin is a thin lamella, and it is to be expected that stresses are continuous and uniform within the twin. If a local coordinate system is defined with axis 1 along the shear direction of the twin system and the 3 direction along the twin plane normal, i.e., with the 1 and 2 axes within the twin plane (see Fig. 1a), the following continuity conditions may be enforced across the twin plane for the elastic strain components:

$$\varepsilon_{11}^{\text{el,parent}} = \varepsilon_{11}^{\text{el,twin}}, \quad \varepsilon_{22}^{\text{el,parent}} = \varepsilon_{22}^{\text{el,twin}} \quad \text{and} \quad \varepsilon_{12}^{\text{el,parent}} = \varepsilon_{12}^{\text{el,twin}} \tag{11a}$$

and for the stress components:

$$\sigma_{33}^{\text{parent}} = \sigma_{33}^{\text{twin}}, \quad \sigma_{23}^{\text{parent}} = \sigma_{23}^{\text{twin}} \quad \text{and} \quad \sigma_{13}^{\text{parent}} = \sigma_{13}^{\text{twin}} \tag{11b}$$

Thus, one is assuming that the elastic strains within the plane of the newly formed twin are compatible (in fact equal) to the matrix on the other side of the twin boundary. Further, one is assuming that stresses acting on the twining plane are also equal across the boundary.

As the elastic stiffness tensor of the twin is known, it is then possible to calculate the remaining six stress and elastic strain components in the twin grain. Since the elastic constants of Mg are nearly isotropic, the conditions (11) practically amount to enforcing the same stress in parent and twin. The initial plastic strain in the twin is assumed to be equal to the current plastic strain in the parent grain, as dislocations present in the parent grain, if any, might also be present within the twin, although in some way transformed by the twinning event itself. It is important to account for the accumulated plastic strain in the newly created twin in order to incorporate effectively the effects of prior strain hardening on subsequent plastic deformation within the twin. As suggested in the discussion of Eq. (1), the activation of a twin system in the parent grain has a similar effect to a slip system: it results in a plastic shear strain $\delta \gamma^{\text{twin}}$ in the parent which induces some stress relaxation in the parent due to the twin activity. The approach described above has been implemented in the EPSC code and is referenced in what follows as the 'Continuity' approach. The only distinctions between this approach and the one previously implemented [7] are (i) rigorously accounting for the effect of twin reorientation on the texture evolution and (ii) determining the initial

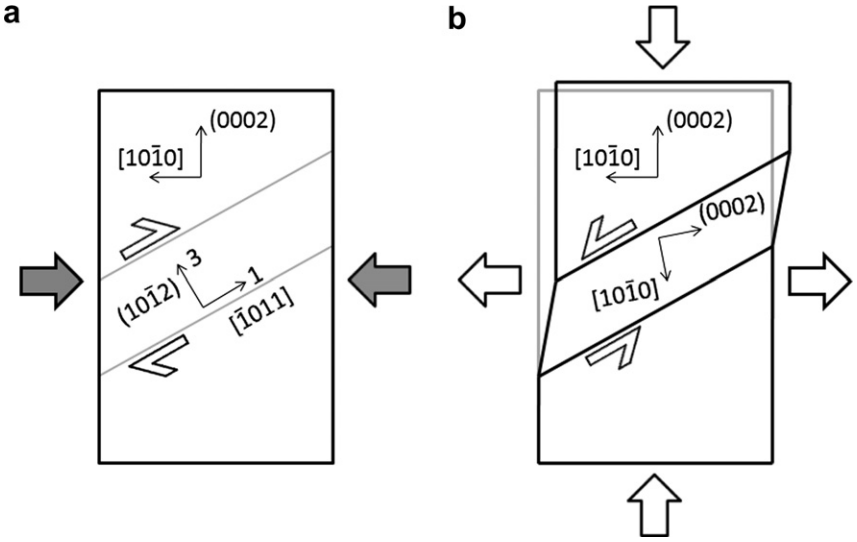

Fig. 1. (a) Schematic of a typical grain in extruded Mg showing the crystallographic elements and the compression direction (shaded arrows); (b) schematic of the tensile twin domain and the medium-induced reaction stresses (arrows) associated with activating a 'FIF'. A 'tensile' reaction component perpendicular to the page (not drawn) is also present.

stress and strain state within the twin (i.e., through Eq. (11)), which are then averaged to calculate the aggregate stress state after the self-consistency relations are satisfied. This latter point becomes important when the initial twin shear is large, as explained below.

In reality, while the conditions for twin nucleation are not well understood, and the condition for initial twin propagation is similar to that of a crack [18]: while a rather large local shear stress is required to destabilize it, the stress for propagation is smaller. As a consequence, once activated, it tends to lower the elastic energy by growing to a more energetically favorable size. This process involves 'overshoot', that is, a larger shear than the one actually required to accommodate the applied deformation. In what follows, an a priori assumption is made of the initial twin size 'at birth' and hence the approach is termed the 'finite initial fraction' (FIF) approach. By assuming that the twin nucleates and grows to a fixed volume fraction f^0 of its parent grain, one is effectively prescribing a fix initial plastic shear for the twin system. This plastic shear is related to the fixed volume through Eq. (9):

$$\gamma^0 = f^0 S^t \tag{12}$$

This 'excess' plastic shear will generate a back-stress between the parent and twin because of the constraint of the surrounding polycrystal. This situation is sketched in Fig. 1a and b, showing schematically the 'before' and 'after' geometry of the twinned grain, and the reaction stress from the surrounding medium opposing the shear. One can estimate this back-stress by assuming that the imposed plastic shear strain results in an equal and opposite elastic shear strain:

$$\varepsilon_{ij}^{0,t} = -m_{kl}^t \gamma^0 \tag{13}$$

where $\varepsilon_{ij}^{0,t}$ is the elastic back-strain in global coordinates, and m_{kl}^t is the Schmid tensor for the twin system. Eq. (13) is equivalent to saying that the parent grain is infinitely stiff compared with the twin and thus not accommodating any of the plastic shear, forcing the twin to develop an equal and opposite elastic strain. Of course, the grain in which the twin appears could accommodate the strain elastically or even elasto-plastically, so the stress relaxation computed by this relation clearly represents an upper-bound approximation. Accepting this limitation for the time being, the back-stress (stress in the inclusion) is found simply as

$$\sigma_{ij}^{0,t} = C_{ijkl}^{\text{twin}} \varepsilon_{kl}^{0,t} \tag{14}$$

where C_{ijkl}^{twin} is the elastic stiffness tensor of the twin. For the parent grain, the stress relaxation is introduced by correcting the current stress with the calculated back-stress weighted by the initial relative size of the twin f^0:

$$\sigma^{\text{parent}} = \frac{\sigma^{\text{parent}} + \sum_t \sigma^{0,t} f^0}{1 - \sum_t f^0} \tag{15}$$

where the sum is made over the twin systems t, which become active in the current step (in symmetrically oriented grains, multiple twin systems may become active in the same step). From a physical point of view, one would expect that the stress in the parent (and specifically the shear component parallel to the twin plane) to relax upon twin activation, and to a larger extent than initially determined through Eqs. (1)–(7) owing to the 'overshoot' argument expressed above (and quantified by Eqs. (12) and (13). When the twin grows beyond the shear required by Eqs. (1)–(7), it induces a reaction stress from the medium, which is opposite to the sense of the twin shear (Fig. 1). By weighting of this reaction by f^0, the stress is 'spread' over the volume of the parent grain. In a simplified way, one is trying to capture simultaneously a twin–parent interaction (for which the authors have referred to a recent FE study [17]) and

a parent–medium interaction. For the latter interaction, it is considered that the localized twin shear is distributed over the whole parent grain. That some plastic relaxation occurs in the vicinity of the twin is undeniable. However, the degree of overshoot f^0 is not firmly established and so the simplicity of the upper-bound model represented by Eq. (13) is attractive at present from the perspective of gaining first-level insight.

Inside the twin, the initial stress state is set equal to the back-stress, and the elastic strain component for the twin is equal to the back-strain. The plastic strain 'inherited' by the twin is set equal to the plastic strain in the parent. In summary, the FIF approach differs from the continuity approach in the assumption used to define the initial stress in the newly formed twin, and by the condition that the twin nucleate with a finite volume fraction. Again, the stress–strain state within the twin nuclei and the update to the parent stress state are incorporated after the self-consistency conditions have been satisfied. The rationale for this approach is the realization that twinning is a sudden event, to which the polycrystal does not immediately respond, and this is what gives rise to the dramatic discontinuities in the grain-level stresses that have been measured using neutron diffraction.

3. Experimental technique

Commercial magnesium alloy AZ31 has a nominal composition of 3 wt.% Al and 1 wt.% Zn, with restrictions on the transition metal impurities Fe, Ni and Cu in order to improve the corrosion resistance of the alloy. A 1.25" (31.75 mm) diameter rod of AZ31 was received from a vendor in the as-extruded condition [14]. The extrusion process results in the so-called rod texture in magnesium alloys, where all the basal poles are oriented nearly perpendicular to the extrusion direction (see Fig. 2). The texture was measured on HIPPO [19], the designated texture instrument at LANSCE (Los Alamos Neutron Science Center), without assuming any symmetry for the produced texture. Cylindrical samples, 10 mm diameter and 24 mm long, were machined from the rod with the compression axis aligned with the extrusion axis. The combination of the initial rod texture, the orientation of the samples with respect to the extrusion axis and the compressive loading results in a scenario where almost all grains are favorably oriented for tensile twinning, as their *c*-axis is subjected to tension by the Poisson strains during compression.

In situ neutron diffraction measurements during the compressive loading were made using the engineering instrument SMARTS [20] located at LANSCE. A schematic of the set-up at SMARTS is shown in Fig. 3. The combination of the two detector banks at ±90° to the incident beam and the sample oriented with the loading direction at 45° to the incident beam allows for the measurement of the longitudinal and transverse lattice strains simultaneously. The elastic lattice strains, calculated from the changes in the peak positions during deformation, are given by

$$\varepsilon^{hkil} = \frac{d^{hkil}}{d_0^{hkil}} - 1 \tag{16}$$

The lattice strains are a measure of the average elastic normal strain in the direction of the scattering vector in grains whose *hkil* lattice plane normal is parallel to the scattering vector. Hence, it does not represent the state within a single grain or the bulk, but an average over a subset of grains which fulfill the Bragg scattering condition for a given reflection. Obviously, the accuracy of all ε^{hkil} measurements depends strongly on the accuracy of the d_0^{hkil} values. However, owing to the texture, some of the diffraction peaks are not initially present in both banks (e.g., the 0002 peak in bank 2) (see Fig. 4), and an alternative method of determining the initial lattice spacing, d_0, is needed for those planes. In this case, the ratio between a given *hkil* peak positions in bank 1 and bank 2 was determined separately for all the peaks present. For an unstressed material that is thermo-elastically isotropic and has not been subjected to prior plastic deformation, this ratio should be the same for all *hkil* peaks. Fortunately, the thermo-elastic anisotropy of magnesium alloys is low [21]. In this case, the standard deviation of the ratio was 2.5×10^{-4}, meaning that the possible error introduced would be on the order of 250 micro-strain (με). This ratio was applied to obtain the lattice parameters for the peaks initially missing in one of the banks. This method was previously used successfully on time-of-flight neutron data by Brown et al. [22]. The macroscopic strain was measured using an extensometer attached to the samples.

Lattice strains were measured as a function of applied stress on two samples; one loaded to a total of ~10% strain and one loaded to a total of ~5% strain. The first sample was held in load control all the time, which led to a large jump in strain between the applied stresses of 120 and 125 MPa (see Fig. 5), once twinning commenced. Hence, the second sample was held in stroke control through the plateau in the stress–strain curve to obtain more detailed data in this region. The time it took to make each neutron measurement was on the order of 20 min. Fig. 5 shows that the samples did experience some creep while held at constant load higher than ~250 MPa. The first sample failed at an engineering stress of 320 MPa. The second sample was loaded in stroke control <2% strain, and this confirmed that the large strain increment at the plateau on the first sample did not change the stress–strain behavior later in the loading cycle.

The initial and final textures were measured on HIPPO [19], and both showed almost perfect axisymmetry (see Fig. 2 for the initial texture, the final one is presented later). This was expected, as both the extrusion process and uniaxial compression are inherently axisymmetric. Such symmetry allows one to use the two diffraction patterns measured from SMARTS to reconstruct the full texture, assuming it is a true axisymmetric texture. Fig. 2 shows the comparison of the initial texture measured on HIPPO without any assumptions, and the initial texture measured on SMARTS

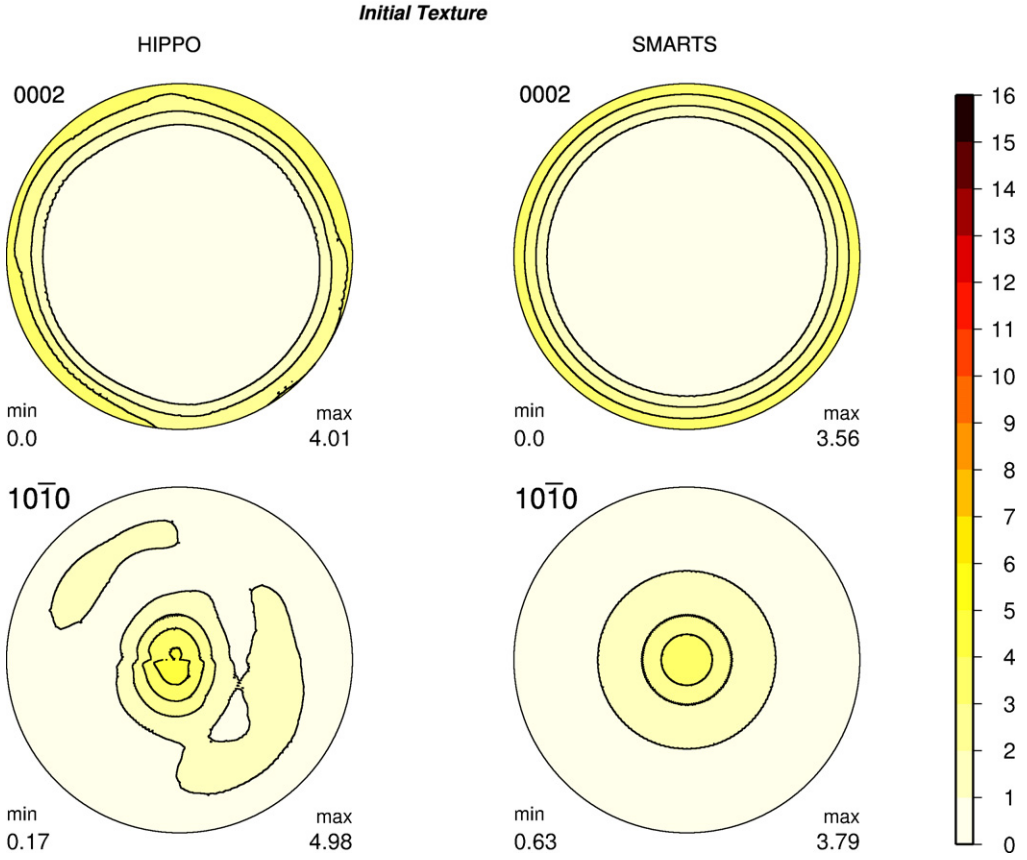

Fig. 2. Initial texture of the extruded magnesium alloy (the extrusion axis is at the center of the pole figures), measured with HIPPO without any symmetry assumptions, and measured with SMARTS assuming fiber symmetry.

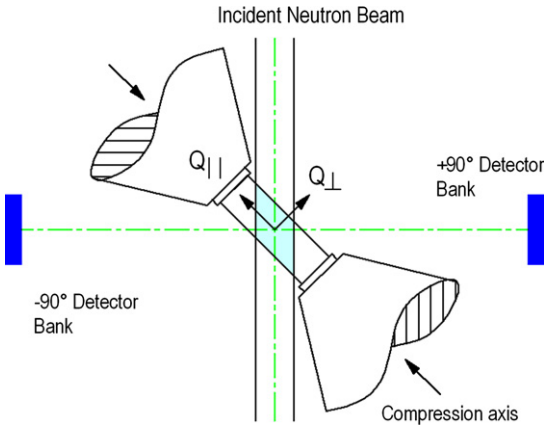

Fig. 3. Schematic of the in situ compression set-up of the SMARTS instrument.

using the fiber texture assumption. The differences between the HIPPO and SMARTS textures are limited to changes in the position of the minima and maxima and a slight decrease in the maxima. This is important, as one can then use the texture determined from SMARTS to determine the twin volume fraction in situ as follows. Axisymmetric textures can be visualized using the axial distribution function (ADF), which is a cut through the pole figure at a line from the center to the perimeter. The evolution of the basal pole ADF (0002) with applied strain is shown in Fig. 6a. Initially there is no basal pole density at the center and then, at strains >2%, the density grows at the center and decreases at the rim. From the ADF, one can calculate the evolution of the 0002 peak density in the longitudinal and transverse directions with applied strain (see Fig. 6b) from the end-points of the curves in Fig. 6a), and one can also calculate the twin volume fraction (see Fig. 6c) by integrating the area under the ADF. In the present case, the ADF is essentially zero at 45° for all strain levels, and thus one can use the ratio of the area under the curve between 0° and 45° and the area under the curve between 45° and 90° as a direct measure of the twin volume fraction. Note that the selection of 45° to be the dividing point for the determination of the twin volume fraction is specific for the present case, and that it is not necessarily appropriate for other textures.

Fig. 6b shows that the 0002 pole densities determined from the texture refinement are in good agreement with the intensities from single peak fits of the same data: initially, there are no grains with their 0002 pole along the loading axis, and there is a high concentration of grains with their 0002 pole perpendicular to the loading axis (~3.5 times random). Notice that the intensities determined from the texture refinement have a meaningful unit, i.e., multiples of random distribution, whereas the

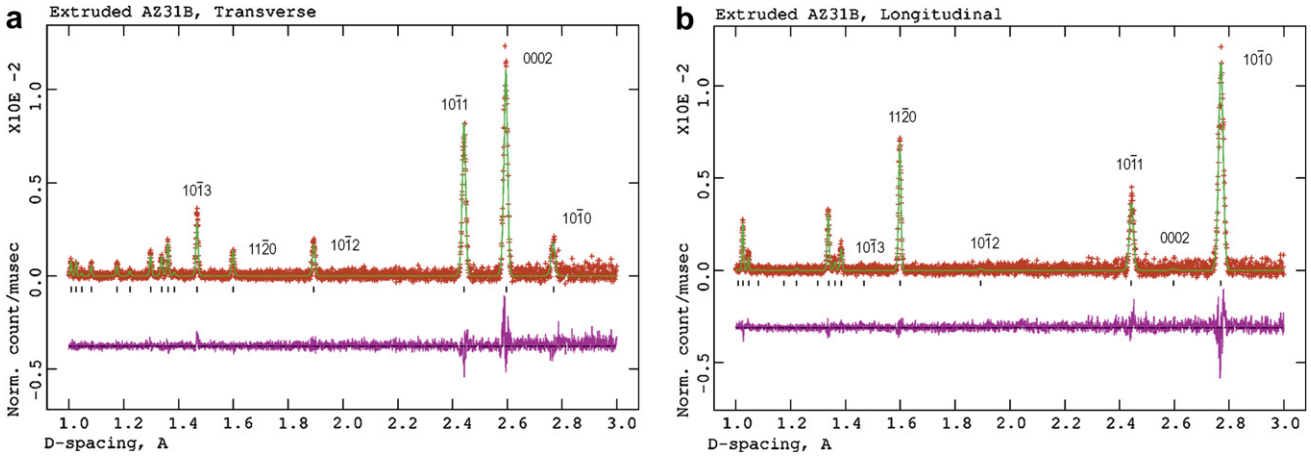

Fig. 4. Diffraction patterns measured on SMARTS: (a) parallel to the loading axis (extrusion axis); (b) transverse to the loading axis. The red crosses are the measured data, the green line is the Rietveld refinement, the magenta line is the difference curve and the black tick marks indicates the hcp reflections, with a few *hkil* given.

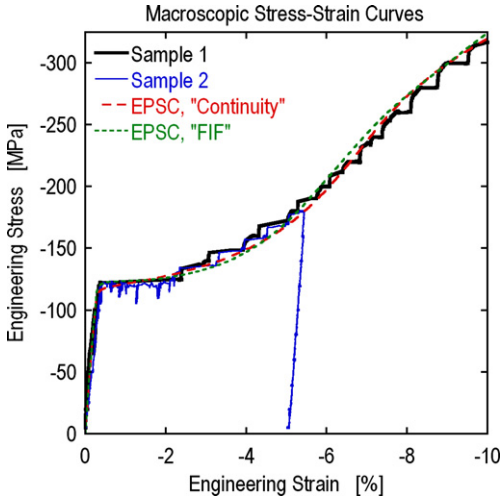

Fig. 5. Measured macroscopic stress–strain curve (load cell and extensometer) for the in situ loading measurements on SMARTS. Sample 1 was loaded entirely in stress control, whereas sample 2 was loaded in stroke control during the initial stage of the plateau. The curves labeled EPSC are calculated using the present model.

single peak fits are in arbitrary units. The concentration of grains with their pole along the loading axis increases rapidly and almost linearly with strain, to a maximum of ~10 times random at 7.4% strain. Subsequently, it decreases slightly to a final value of ~8.5 times random at 10% strain. The twin volume fraction determined from the measured textures is shown in Fig. 6c. Notice that 70% of the polycrystal has undergone twinning after only 10% strain.

4. Experimental results

The measured lattice strains for the $10\bar{1}0$, 0002, $10\bar{1}1$ and $11\bar{2}0$ reflections are shown in Fig. 7. Data were refined for more reflections, but only these four are shown here for clarity. Also, lattice strain data were collected from both the load and stroke control samples but, for clarity, only the four aforementioned reflections for the first sample and the 0002 reflection for the second sample are shown.

For the longitudinal direction (Fig. 7a), it is clear that, when the 0002 peak becomes large enough to fit, at about −120 MPa, the lattice strain of the twins is far into tension. As discussed earlier, the uncertainty in determining the d_0 is on the order of 250 με, so the observed positive 2000 με is truly indicative of a significant tensile stress state in the newly formed twins. This effect is also reflected in the transverse data (Fig. 7b), where it is seen that the 0002 reflection jumps to almost zero elastic lattice strain at −120 MPa where twinning starts, and in this direction there is no ambiguity regarding d_0 or low peak intensity, as the 0002 reflection is initially strong in the transverse direction. To emphasize further that the large jumps are not due to the fact that sample 1 was loaded in load control, the 0002 data from sample 2 is overlaid in Fig. 7 with open symbols. The lattice strain data from sample 1 and 2 (load and stroke control, respectively) are consistent within the uncertainty in the measurement of d_0.

In general, all the peaks with a *c*-component (only 0002 and $10\bar{1}1$ are shown here) exhibit strong non-linear behavior initiating at an applied stress of −120 MPa, indicating that significant stress redistribution takes place as twinning begins. It is also worth noting that the $10\bar{1}1$ reflection in the longitudinal direction shows non-linearity very early, which can be linked to early basal slip activity. This was previously discussed in Ref. [14].

5. Modeling results

Previous studies of Mg AZ31 using EPSC modeling and neutron diffraction show good agreement between measured and calculated internal strains when the contribution of twinning to plastic deformation is minimal [11,14]. However, in the present case of compressive loading of

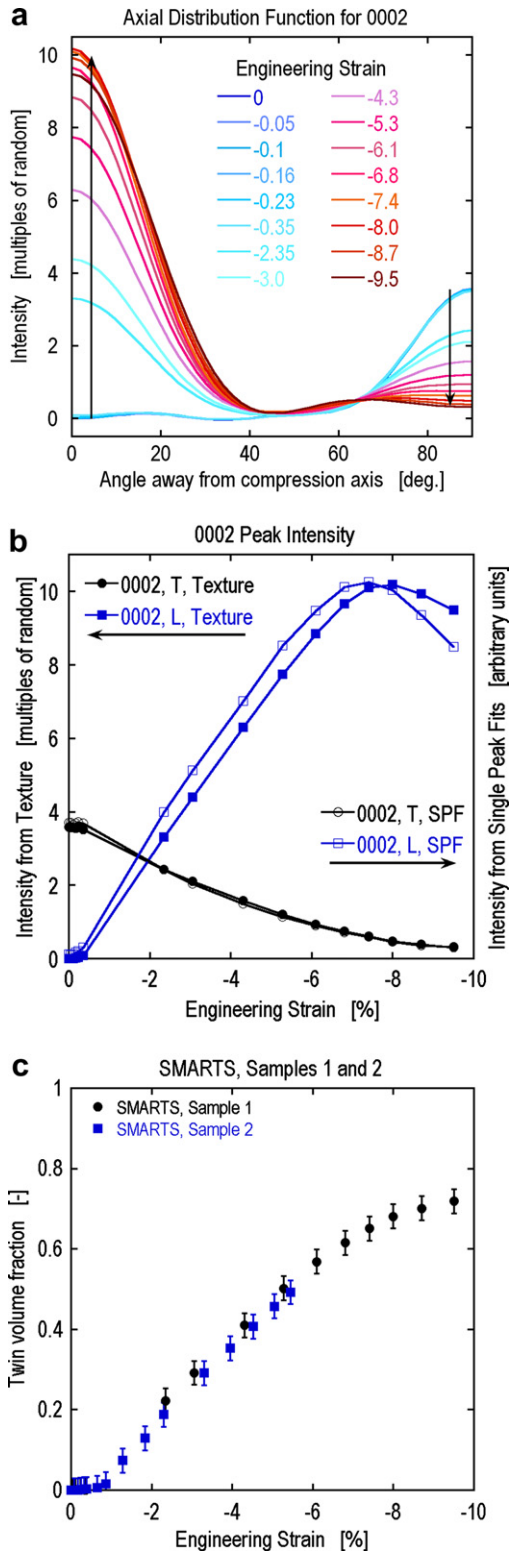

Fig. 6. (a) Measured ADFs determined from the SMARTS diffraction data assuming fiber symmetry as a function of engineering strain. Notice the large jump in strain between −0.35% and −2.35%. (b) 0002 peak intensity as a function of engineering strain; extracted from the 0002 poles shown in (a) and from single peak fits. (c) Twin volume fraction obtained by integrating the area under the curves in (a).

extruded magnesium alloy, the original twinning scheme in the EPSC model is not capable of predicting either the macroscopic stress–strain curve or the internal lattice strains. Using the present twinning scheme that explicitly takes into account the texture development due to twinning, it is possible to obtain good agreement between the calculated and measured macroscopic stress–strain curves applying either of the two assumptions described above ('Continuity' or 'FIF') (see Fig. 5). This result underlines the importance of accounting for geometric texture hardening when twinning is a major contributor to deformation, which has also been noted by Barnett et al. [23]. It will be shown in what follows, however, that comparison of the internal strain, measured and calculated, does discriminate between the two model assumptions, in favor of the FIF.

The present calculations have included the slip and twinning modes used in Ref. [14] to analyze the tensile data of extruded magnesium alloy; basal slip $\{0001\}\langle 2\bar{1}\bar{1}0\rangle$, prism slip $\{10\bar{1}0\}\langle\bar{1}2\bar{1}0\rangle$, second-order pyramidal slip and tensile twinning $\{10\bar{1}2\}\langle\bar{1}011\rangle$. It was concluded in Ref. [14] that prismatic and pyramidal $\langle a\rangle$ slip induce similar effects. As a consequence, the latter is not included in what follows. The activity of each deformation mode is governed by critical resolved shear stress (CRSS) values, and the evolution of the CRSS with accumulated shear is determined using a Voce-type hardening law as described earlier (see Eq. (4)). The initial CRSS values and the parameters of the Voce hardening law were used to fit the predicted macroscopic stress–strain curve to the measured one. The different plots in two calculated curves, labeled 'Continuity' and 'FIF', correspond to the two different assumptions used for determining the initial stress and strain state in the twins. For the second assumption, the initial twin fraction f^0 was used as a fitting parameter, and chosen to reproduce the initial tensile elastic strain in the newly formed twins. Note that relaxing the assumption of Eq. (13) to include plastic accommodation of the twin shear by the matrix would result in higher values of f^0. The values of the CRSS, hardening parameters and initial twin fraction are given in Table 1.

Comparing the results of the 'Continuity' calculations with the measured elastic lattice strains, it is evident that the model qualitatively predicts the strong non-linear behavior of the measured internal strain data (see Fig. 8a and b). The changes in the slopes seen at the onset of twinning are predicted well, especially the reversal of the slope for the $10\bar{1}1$ and 0002 reflections in the transverse direction. However, the continuity assumption does not predict the large jump in lattice strain observed for several of the reflections, and particularly for the 0002, at the onset of twinning. Also, it is worth noting that the prism reflections, $10\bar{1}1$ and $11\bar{2}0$, are not well predicted in the transverse direction. These grains appear either to have a too large Poisson's ratio or to be subjected to large transverse tension in the calculations. The early non-linearity of the $10\bar{1}1$ reflection in the longitudinal direction is well predicted by the model. This feature is only achievable if the CRSS for basal slip is very low.

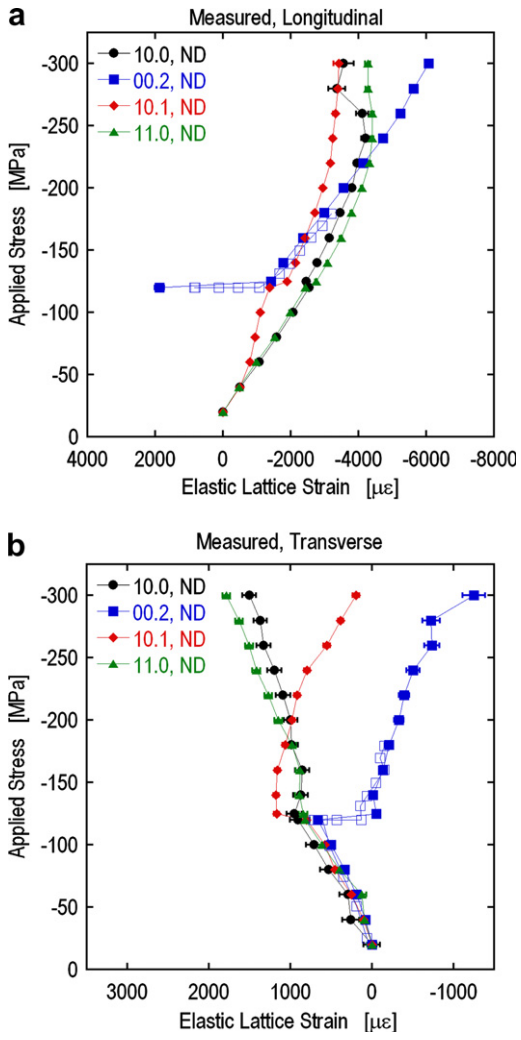

Fig. 7. Measured elastic lattice strains versus applied stress: (a) parallel to the loading axis; (b) perpendicular to the loading axis. Solid symbols are for sample 1 (loaded in stress control) and the open symbols are for sample 2 (loaded in stroke control through the plateau). Only the 0002 reflection from sample 2 is shown for clarity.

Table 1
CRSS and hardening parameters used for the two assumptions

Assumption	Initial twin fraction	Deformation system	τ_0 (MPa)	τ_1 (MPa)	θ_0 (MPa)	θ_0 (MPa)
Continuity	N/A	Basal	12	20	40	0
		Prism	60	20	40	0
		Pyramidal	100	117	2500	0
		Tensile twin	54	0	0	0
Fixed initial fraction	3%	Basal	12	20	240	0
		Prism	60	20	240	0
		Pyramidal	100	117	2000	0
		Tensile twin	60	0	0	0

Fig. 8c and d presents the striking results obtained when using the FIF assumption. The large jumps 0002 observed for the reflection in both directions are reproduced, and also the jump and slope-reversal for the $10\bar{1}1$ in the transverse direction is reproduced. Most of the reflections are in excellent qualitative agreement with the measurements: almost quantitative agreement. The behavior of the $10\bar{1}0$ and $11\bar{2}0$ reflections in the transverse direction, however, is still puzzling. It is clear from the pole figures in Fig. 10 that the prism planes that contribute to diffraction in the transverse direction belong, initially, to the parent grains and, as deformation proceeds, that diffracting line is increasingly associated with the twinned domains. The schematic representation in Fig. 1b indicates that the excess twin shear will induce a tensile component normal to $10\bar{1}1$ and a compressive component normal to $11\bar{2}0$. In addition, it is likely that the reaction stresses will continue to play a role in twin and parent throughout twinning activity. As a consequence, the assumption of treating the twin as a separate grain once formed may be disregarding the fact that the stress relaxation that takes place in the parent grain due to the twin shear affects the stress state in the twin. To pursue this effect could involve development of a multiple-site EPSC code [24] and is not within the scope of the present work.

A comparison of the measured ex situ and predicted textures based on the FIF assumption at 0%, 5% and 10% deformation is shown in Fig. 9 for the 0002 and $10\bar{1}0$ pole figures. The measured initial texture shows a high concentration along the rim of the 0002 pole figure and a matching high concentration at the center of the $10\bar{1}0$ pole figures, characteristic of the rod texture of the extruded magnesium alloy. The discretized initial texture contains 15,548 orientations and reproduces in detail the measured initial texture. This shows that the discretization of the measured texture is sound. After 5% deformation, the density increases at the center of the 0002 pole figure and decreases at the rim. The reverse is observed for the $10\bar{1}0$ pole figure where density increases at the rim and decreases at the center. This is a clear signature of tensile twinning, where the orientation of the basal pole changes by 86.6°.

At 10% deformation, the trend has continued, and now the maximum 0002 density is at the center of the $10\bar{1}0$ pole figure, and the density in the pole figures is concentrated at the rim. The predicted textures at 5% and 10% deformation are also in very good agreement with the measured textures. Only the predicted density at the center of the 0002 pole figure is too high compared with the measured density. In fact, looking at the texture determined by in situ neutron diffraction measurements on SMARTS assuming cylindrical symmetry (see Fig. 2a and b), it is clear that the measured density at the center of the 0002 pole figure is actually decreasing after ~8% deformation. The model predictions indicate that this is just about the point where pyramidal $\langle c+a \rangle$ slip becomes the dominant deformation mode in the twinned grains. Hence, the decrease in 0002 density at the center is most likely due to pyramidal slip activity that is known to reorient basal planes away from the compression axis

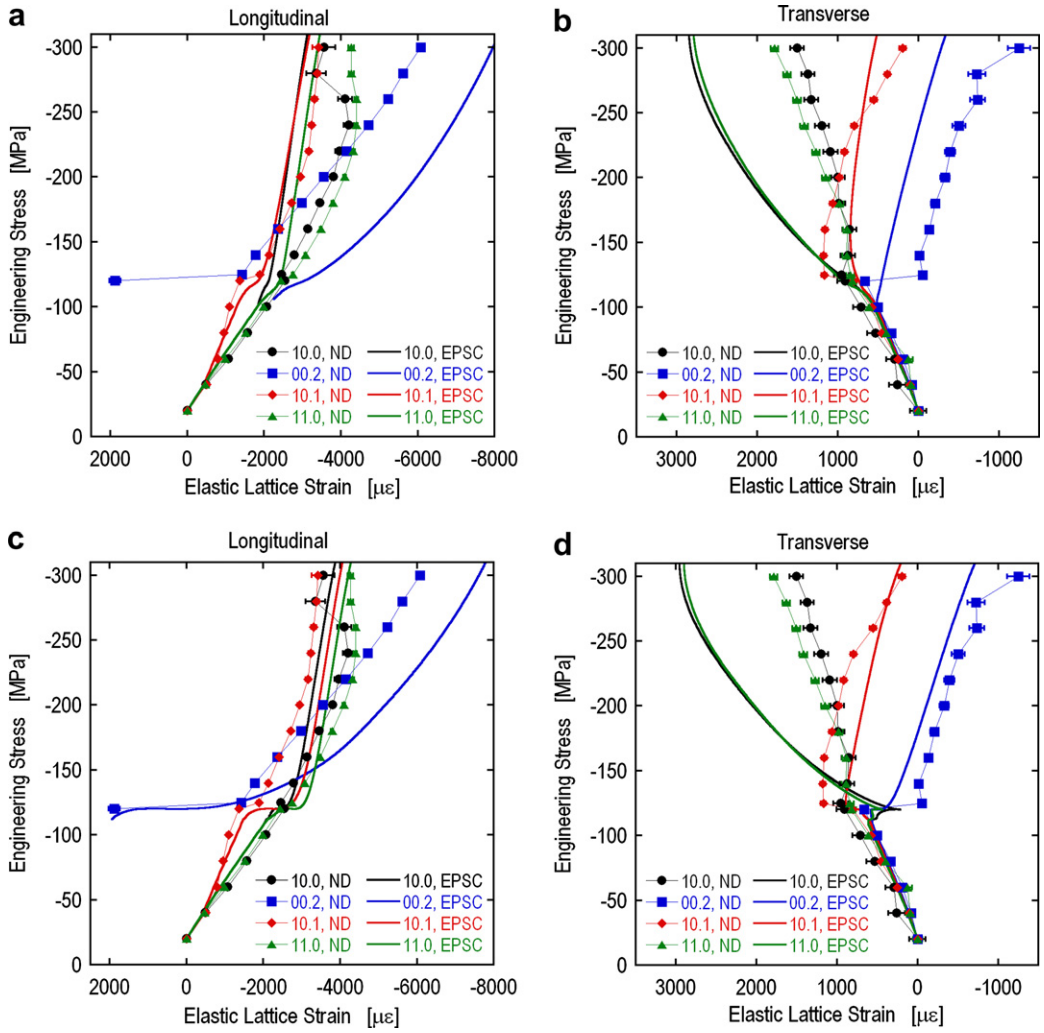

Fig. 8. Measured (line and symbol) and predicted (thick line) elastic lattice strains for the 'Continuity' assumption: (a) parallel to the loading axis; (b) perpendicular to the loading axis; and for the 'FIF' assumption: (c) parallel to the loading axis; and (d) perpendicular to the loading axis.

[25]. In the present implementation, the EPSC model does not take into account the texture development due to crystallographic slip, and this is likely the cause of the too high 0002 density along the compression axis at higher strains.

The measured and predicted twin volume fractions are compared in Fig. 10. It is clear that the model predicts a slightly lower final twin volume fraction than was measured. For the 'FIF' assumption, the twin volume fraction increases rapidly at the onset of twinning owing to the prescribed 3% minimum twin fraction, but it approaches the prediction of the 'Continuity' assumption at higher strains.

The CRSS and hardening parameters used in the calculations are given in Table 1. The parameters that were changed to accommodate the two assumptions are highlighted by a gray background. The increase in the initial hardening slope θ_0 for the basal and prism systems for the 'FIF' assumption is needed owing to the stress relaxation that would otherwise result in an actual stress drop right after twinning starts. However, as the transition range between initial and final hardening, given by τ_1, is very limited, it only affects the very early stages of activity on these systems.

The system activities as a function of strain are shown in Fig. 11 for both assumptions. Note the bi-linear strain axis created to highlight the changes within the first 1% strain. It is clear that there are only a few differences between the activities in the parent grains (the thick dashed lines), depending upon the assumption used for the determination of the initial state in the twins, the main difference being the slightly lower initial fraction of twin activity for the FIF assumption. Similarly, there is only one major difference for the twin grains, but it is a very important difference: for the Continuity assumption (Fig. 11a), the basal system is active in the twin grains as soon as they appear, whereas there is a gap of >0.3% strain between the onset of twinning and the onset of any slip activity in the twin grains for the FIF assumption (Fig. 11b). This is due to the stress relaxation included in the FIF assumption. At higher strains, the behavior is almost the same for the two assumptions: almost steady state in the parent grains with

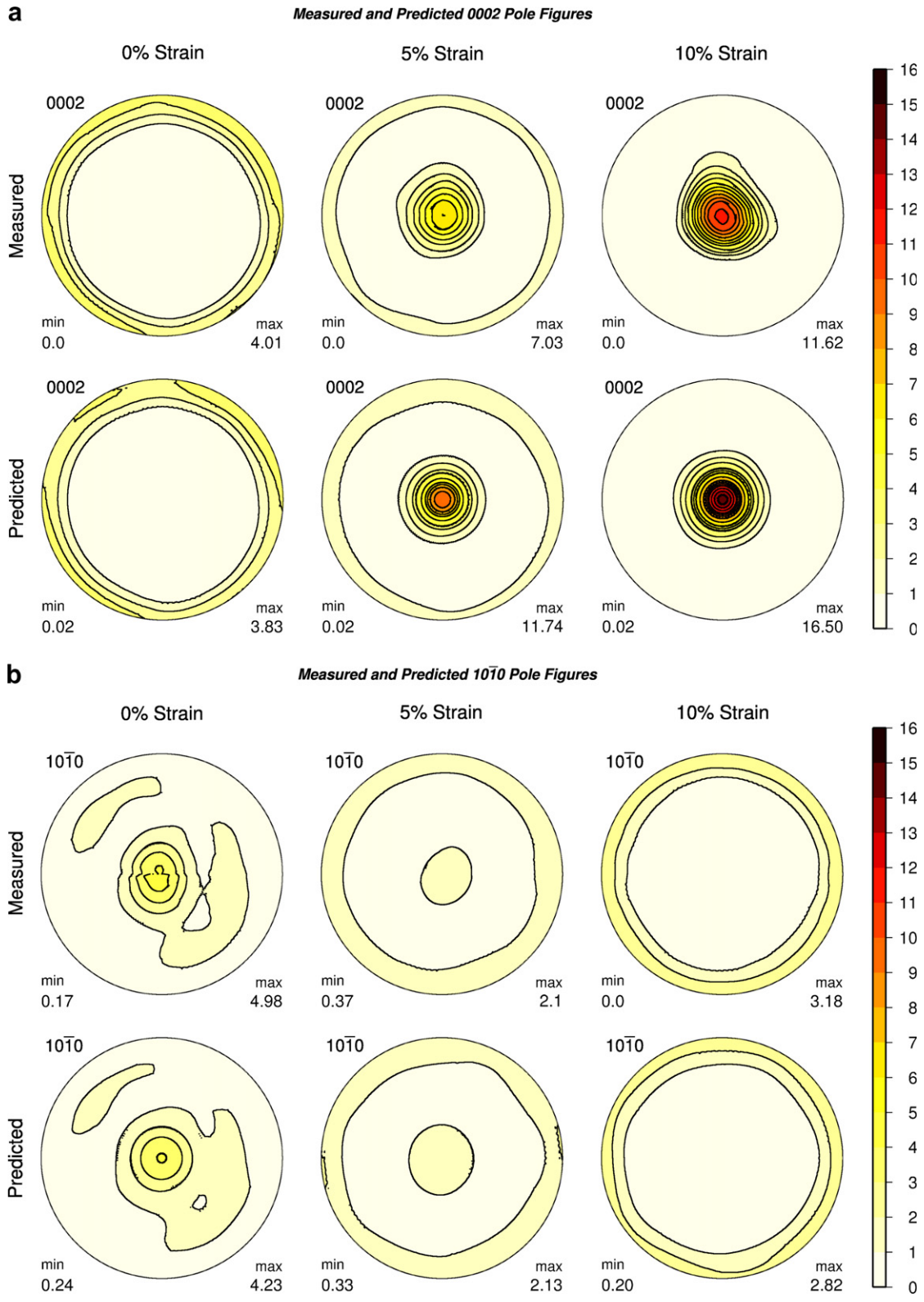

Fig. 9. Measured (HIPPO) and predicted ('FIF' assumption) basal and prismatic pole figures.

very little pyramidal activity, and a switch between basal dominating to pyramidal dominating in the twins with very little prism activity. The fully elastic behavior of the twins immediately after they are created, i.e., lack of system activity, seen for the FIF assumption is consistent with the very shallow initial slope measured for the longitudinal 0002 reflection which indicate that the twins are initially loading elastically.

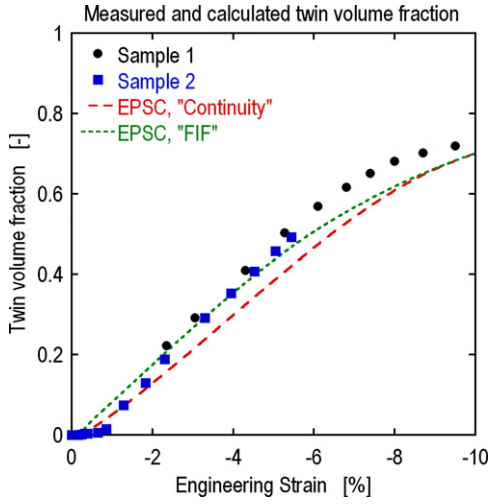

Fig. 10. Measured and predicted twin volume fractions.

6. Conclusions

Several features are very distinctive in materials where twinning makes a substantial contribution to plastic deformation. They are: a very rapid texture development associated with twin reorientation; an unusual hardening response; and abrupt stress relaxation inside those grains undergoing twinning. In the extruded Mg AZ31 studied here, the characteristic rod texture combines with the symmetry of compression along the rod axis, to demand *c*-axis extension in a majority of grains. The in situ measurements of internal stress evolution reveal a highly non-linear and non-monotonic response, with signs of stress inversion in some orientations, which is obviously correlated with twinning. What is less obvious is the precise role that slip and twinning mechanisms, plus the grain to grain interactions, play in such behavior. All of the above motivated the authors to extend the EPSC model, an elasto-plastic self-

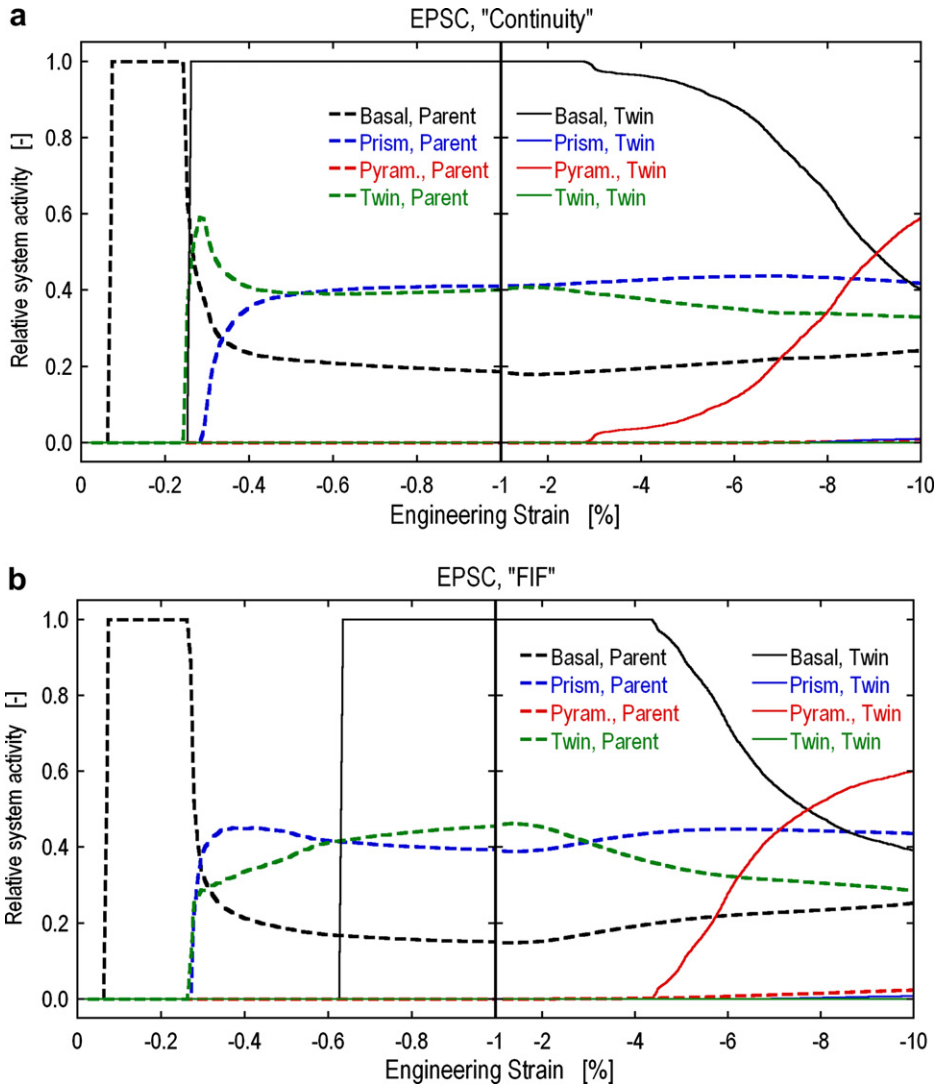

Fig. 11. Predicted relative system activity: (a) 'Continuity' assumption and (b) 'FIF' assumption. The thick dashed lines are for the parent grains and the thin solid lines are for the twin grains. Note the bi-linear strain axis; the first half of the plots highlights the initial range from 0% to 1% strain, and the last half of the plots show the range from 1% to 10% strain.

consistent polycrystal approach used successfully in the past to interpret neutron diffraction, to account for the relevant features of this problem.

The authors allowed for creation and growth of new twin grains with strain, while the parent grain's volume fraction concomitantly decreases. This feature alone allowed the evolution of yield stress, texture and twin volume fraction with strain to be predicted correctly, which could not be accomplished with previous models. The qualitative agreement between experiments and model predictions is excellent for all of the above. However, accounting for the texture evolution associated with twinning alone is not sufficient for a satisfactory prediction of the internal stress evolution. For this reason, it was hypothesized that twin creation is associated with an instability of the system caused by a rapid decrease in stored elastic energy. This process is accompanied by a redundant twin shear upon twin nucleation and a sharp local stress reversal in the parent and twin. Incorporating the FIF assumption into the model caused the agreement with the measured data to improve significantly, giving evidence that this is the process taking place in the real material. In this work, the FIF was taken to be 3% of the parent grain volume, as this resulted in good agreement with the measured diffraction data. It is also consistent with detailed FE method calculations of the local stresses and strains during twinning in zirconium presented by Zhang et al. [17], which are based upon energy minimization. However, it should be noted that the current value of 3% should be regarded as a minimum value, owing to the upper-bound assumptions made in determining the back-stress in the twin. Neither of the assumptions presented here for the updated EPSC model was able to predict accurately the lattice strains for the prism poles $10\bar{1}0$ and $11\bar{2}0$ in the transverse direction. The authors believe that this is due to the lack of direct interaction between the parent and twin grains subsequent to twin formation. Planned future development of a two-site EPSC model or a composite grain formulation may shed further light on this issue.

One of the other outstanding questions from previous work [14] was the inability of the previous EPSC model to reproduce the tension–compression asymmetry of the yield point. The present implementation of the EPSC model still does not enable a single set of CRSS and hardening parameters to fit both tension and compression behavior simultaneously and precisely, although the present model does fit the data better than the previous model and does enable all the salient features of twinning-dominated compression behavior to be captured, as discussed. The major outstanding issue, in this regard, is the fact that the CRSS for the prism slip system has to be increased 50% (from 60 to 90 MPa) to reproduce the higher yield point in the experimental tensile data. Notably, this is very similar to the CRSS values obtained using the previous model [14]. This requirement to change the CRSS of prismatic slip may indicate a non-Schmid effect on the $\langle a \rangle$ dislocation core as has been suggested for titanium alloys [26].

Acknowledgement

This work was funded by the Office of Basic Energy Science (DOE) through Project FWP 06SCPE401. This work has benefited from the use of the Lujan Neutron Scattering Center at LANSCE, which is funded by the Office of Basic Energy Sciences (DOE). Los Alamos National Laboratory is operated by Los Alamos National Security LLC under DOE Contract DE-AC52-06NA25396.

References

[1] Jain A, Agnew SR. In: Proceedings of the TMS 2006 annual meeting – magnesium technology, San Antonio, TX; March 12–16 2006. p. 219–24.
[2] Hutchinson JW. Proc Roy Soc Lond 1976:101–27.
[3] Lebensohn RA, Tomé CN. Acta Metall 1993:2611–24.
[4] Proust G, Tomé CN, Kaschner GC. Acta Mater 2007:2137–48.
[5] Tomé CN, Kaschner GC. Mat Sci Forum 2005:1001–6.
[6] Hutchinson JW. Proc Roy Soc Lond 1970:247–72.
[7] Turner PA, Tomé CN. Acta Metall 1994:4143–53.
[8] Clausen B, Lorentzen T, Leffers T. Acta Mater 1998:3087–98.
[9] Eshelby JD. Proc Roy Soc Lond 1957:376–96.
[10] Clausen B, Lorentzen T. Met Trans A 1997:2537–41.
[11] Agnew SR, Tomé CN, Brown DW, Holden TM, Vogel SC. Scripta Mater 2003:1003–8.
[12] Pang JWL, Holden TM, Turner PA, Mason TE. Acta Mater 1999:373–83.
[13] Brown DW, Bourke MAM, Clausen B, Holden TM, Tomé CN, Varma R. Met Trans A 2003:1439–49.
[14] Agnew SR, Brown DW, Tomé CN. Acta Mater 2006:4841–52.
[15] Hill R. J Mech Phys Solids 1965:89–101.
[16] Partridge PG. Metall Rev 1967:169–94.
[17] Zhang RY, Daymond MR, Holt RA. Mat Sci Eng A 2008:139–46.
[18] Lebensohn RA, Tomé CN. Phil Mag A 1993:187–206.
[19] Matthies S, Pehl J, Wenk HR, Lutterotti L, Vogel SC. J Appl Cryst 2005:462–75.
[20] Bourke MAM, Dunand DC, Üstündag E. Appl Phys A 2002:S1707–9.
[21] Touloukian YS. Thermophysical properties of matter. Thermal expansion, vol. 12. New York: IFI/Plenum; 1975.
[22] Brown DW, Agnew SR, Bourke MAM, Holden TM, Vogel SC, Tomé CN. Mat Sci Eng A 2005:1037–42.
[23] Barnett MR, Davies CHJ, Ma X. Scripta Mater 2005:627–32.
[24] Daymond MR, Preuss M, Clausen B. Acta Mater 2007:3089–102.
[25] Agnew SR, Yoo MH, Tomé CN. Acta Mater 2001:4277–89.
[26] Neeraj T, Savage MF, Tatalovich J, Kovarik L, Hayes RW, Mills MJ. Phil Mag 2005:279–95.